Journal of Computational Physics **161,** 576–588 (2000)
doi:10.1006/jcph.2000.6514, available online at http://www.idealibrary.com on IDEAL®

COBRA: An Optimized Code for Fast Analysis of Ideal Ballooning Stability of Three-Dimensional Magnetic Equilibria

R. Sanchez,*,[1] S. P. Hirshman,* J. C. Whitson,* and A. S. Ware†

**Oak Ridge National Laboratory, P.O. Box 2009, Oak Ridge, Tennessee 37831-8070; †Department of Physics and Astronomy, University of Montana, Missoula, Montana 59801*

Received June 22, 1999; revised March 13, 2000

A new, fast, and accurate numerical algorithm to assess stability against ideal ballooning modes in general three-dimensional magnetic configurations of interest to controlled thermonuclear fusion is described. The code for ballooning rapid analysis (COBRA) performs this assessment by solving an eigenvalue problem in the form of a linear second-order ordinary differential equation along magnetic field lines in the configuration. An initial approximation for the eigenvalue is obtained from a fast second order matrix method. In COBRA, this approximate eigenvalue is further refined using a variational principle to obtain fourth-order convergence with the mesh size. Richardson's extrapolation is then applied to a sequence of eigenvalues to estimate the exact eigenvalue using the coarsest possible mesh, thus minimizing the computational time. © 2000 Academic Press

Key Words: stellarators; magnetohydrodynamics; ballooning instabilities; growth rate; spectrum of Stürm–Liouville operators; Richardson's extrapolation.

1. INTRODUCTION

The pursuit of a compact design for a low-cost stellarator fusion reactor has necessitated an understanding of the magnetohydrodynamic (MHD) properties for fully three-dimensional (3-D) configurations. The lack of symmetry of these designs makes unavoidable the use of powerful and sophisticated numerical codes as analysis tools. The optimization of such configurations from the standpoint of stability, reduced particle transport, and engineering feasibility is an open problem that has been the object of intense investigations in the last few years [1–3]. Several compact stellarator configurations based on the concept of quasi-omnigeneity [4] (quasi-omnigeneous stellarator, QOS) and showing good particle transport

[1] Universidad Carlos III de Madrid, Avda. de la Universidad 30, Leganes, 28911 Madrid, Spain.

have recently been obtained using an optimization scheme in which the shape of the outer magnetic surface is varied within a Levenberg–Marquardt optimization loop, using the VMEC 3-D equilibrium code [5] at each iteration to recalculate the magnetic field in the plasma [6, 7]. The plasma thermal energy that can be confined in these configurations, characterized in terms of $\beta \equiv 2p/\mu_0 B^2$ (the ratio of plasma to magnetic energy), is known to be limited by the onset of unstable kink and ballooning modes [8]. The analysis of ballooning stability has until now been carried out only after the completion of the optimization procedure. This is because of the large amount of computational time required by the present ballooning codes (for instance, TERPSICHORE [9] or 3DBALLOON [10]). Often, this analysis reveals that the route towards improved transport taken by the optimizer points to a more ballooning unstable region in parameter space with values of β much smaller than would be desirable for a reactor. The ballooning algorithm described here is sufficiently fast and efficient to be used for these optimization calculations.

The ballooning stability problem can be formulated by an ordinary linear second-order differential equation with nonconstant coefficients representing the balance of stabilization caused by magnetic field line bending and the drive of unfavourable curvature [11–13]. The boundary conditions imposed on the solution render the spectrum of eigenvalues, which are proportional to the square of the growth rate for the ballooning mode. These eigenvalues can be obtained numerically either by integration along a field line or by using trial functions to minimize the related variational principle. For 3-D geometries, the computational time increases linearly with the number of grid points along a field line because most of the calculation is spent evaluating the nonconstant coefficients. Thus, the key to accelerating this calculation is, in addition to a more efficient integrator or minimizer, determining at run time for the coarsest possible grid that can be used to obtain the eigenvalue within a predetermined tolerance. The *co*de for *b*allooning *r*apid *a*nalysis (COBRA) performs this task by combining an efficient field-line integration scheme with the variational approach to achieve quartic mesh convergence for the eigenvalue. Then, Richardson's deferred approach to the limit [14, 15] is used to extrapolate the eigenvalue from a few evaluations on coarse but increasingly finer meshes to the continuous limit.

The paper is organized as follows. Section 2 briefly reviews both the ballooning equation and the related variational principle. The algorithm is then described in detail in Section 3, the matrix method used to preliminarily obtain the eigenvalue is described in Subsection 3.1, and the variational refinement of the growth rate is determined in Subsection 3.2. Richardson's extrapolation scheme is discussed in Subsection 3.3, and Subsection 3.4 describes the method for estimating the integration box size. Some numerical results demonstrating both the accuracy and speed of the new algorithm are presented in Section 4 for a 3-D QOS configuration.

2. THE IDEAL BALLOONING EQUATION

Let us consider a magnetic equilibrium with closed surfaces labeled by an arbitrary radial coordinate s and nested around a central magnetic axis (corresponding to $s = 0$). Introducing generalized toroidal and poloidal angles, ζ and θ, such that the magnetic field lines are straight [16], ideal ballooning stability can be analyzed solving a linear second-order ordinary differential equation of the type [11, 12]

$$[L_0(y) + \lambda R(y)]F = 0, \tag{1}$$

along any field line on every magnetic surface, with the operator L_0 defined as

$$L_0(y) \equiv \frac{\mathrm{d}}{\mathrm{d}y}\left[P(y)\frac{\mathrm{d}}{\mathrm{d}y}\right] + Q(y), \tag{2}$$

with both $P(y)$ and $R(y)$ strictly positive. The asymptotic behavior of the ballooning coefficients is given by

$$\begin{gathered} P(y),\ R(y) \sim y^2, \qquad Q(y) \sim y \\ y \to \pm\infty. \end{gathered} \tag{3}$$

The independent variable y is the normalized length along the magnetic field line. Its initial value, $y = 0$, can be chosen to correspond to any prescribed position on the magnetic surface. The eigenvalue λ is then determined by requiring the solution F to be integrable in $y \in (-\infty, +\infty)$. The spectrum of Eq. (1) is complicated [13, 17, 18]. Because of the self-adjointedness of Eq. (1), its spectrum is real and bounded from below, containing a discrete part (which may be empty) followed by a continuous part, where the solution, no longer integrable, remains bounded. Since $\lambda \equiv -\gamma^2$, where γ is the growth rate of the ballooning mode, the equilibrium is unstable if some negative eigenvalue λ exists in the discrete part of the spectrum for any choice of the initial position.

This eigenvalue problem can also be easily cast in the form of a variational principle defining the functional over the space of all integrable functions [18]

$$\lambda(F) \equiv -\frac{\langle F, L_0(y)F\rangle}{\langle F, R(y)F\rangle}, \tag{4}$$

where the notation

$$\langle G, F\rangle \equiv \int_{-\infty}^{+\infty} G^*(y)F(y)\,\mathrm{d}y \tag{5}$$

has been introduced. The Euler–Lagrange equation [19] resulting from the minimization of Eq. (4) is precisely Eq. (1). Therefore, its global minimum, λ_0, coincides with the lowest eigenvalue in the discrete spectrum of Eq. (1). In the same way, the integrable function F_0 satisfying

$$\lambda(F_0) = \lambda_0 \tag{6}$$

is the eigenfunction associated with this eigenvalue.

3. DESCRIPTION OF THE ALGORITHM

As mentioned in Section 1, the computational bottleneck of any ballooning code is the costly evaluation in terms of CPU time of the coefficients P, Q, and R in Eq. (1) and Eq. (4) at the grid points along the magnetic field line. These coefficients are functions of the magnetic field through $|B|$ and the metric elements of the coordinate transformation from the straight-line system to standard cylindrical coordinates (R, ϕ, Z). These quantities are calculated by the VMEC equilibrium code and are supplied to the ballooning code in the form of the coefficients of an odd (O) or even (E) Fourier series (stellarator symmetry constrains the allowable parities),

$$E(s,\theta,\zeta) = \sum_{m,n} E_{mn}(s)\cos(m\theta - n\zeta) \tag{7}$$

$$O(s,\theta,\zeta) = \sum_{m,n} O_{mn}(s)\sin(m\theta - n\zeta). \tag{8}$$

Because of the complex geometry of the configurations of interest, mode convergence studies show that generally a large number of modes for $|B|$, R, Z, and $\rho \equiv \phi - \phi_s$ ($\phi_s = \zeta$ is the toroidal angle in which magnetic field lines are straight) have to be retained in these series (typically 500 to 1000 modes; this is in contrast to axisymmetric configurations such as the tokamak, for which much fewer modes, typically less than 100, are sufficient). This large number is a consequence of the use of straight-field-line magnetic coordinates. (Non-straight magnetic coordinates, like those used in the equilibrium calculation, appear to be better-suited for this type of calculation. However, the derivation of Eq. (2) then becomes more complicated; the algebraic (straight line) description of magnetic field lines must be replaced by a differential equation relating the poloidal and toroidal angles. Ballooning calculations in which such coordinates are used are envisioned as future upgrades of COBRA.)

The Fourier inversion of these series inside the ballooning code is therefore responsible for most of the computing time used (up to 95% of the time for the typical number of grid points used in existing codes). Because the number of Fourier inversions increases linearly with the number of grid points, the efficiency of the calculation may be improved by (1) using a fast solver (for a given number of points), and (2) determining at run time the minimum number of grid points required to obtain the eigenvalue within a prescribed accuracy.

In COBRA, the efficient solver is a finite-difference matrix scheme (described in Subsection 3.1) that allows a rapid evaluation of the eigenvalue to second order in the y-mesh spacing. This eigenvalue is subsequently refined to fourth order using the variational principle (Subsection 3.2). Richardson's extrapolation scheme (Subsection 3.3) is then used to estimate the infinite-mesh limit for the eigenvalue using the current mesh. This process is iterated using finer meshes until the extrapolation error falls below a prescribed tolerance.

3.1. *Finite-Difference Matrix Scheme*

Before discretizing Eq. (1), a large but finite integration box $[-a, a]$ along the field line is chosen, with $a > 0$ sufficiently large to ensure that the effect on the computed lowest eigenvalue of a further increase of the box size is negligible. Criteria for selecting a are given in Subsection 3.4. Assuming now an odd number of points, N, both full and half meshes are defined as

$$\begin{aligned} y_j &= -a + h(j-1), \qquad j = 1, N \\ y_{j+1/2} &= -a + h(j - 1/2), \qquad j = 1, N-1, \end{aligned} \tag{9}$$

where the step size h is defined as

$$h \equiv \frac{2a}{N-1}. \tag{10}$$

The ideal ballooning equation is then discretized using a centered second-order, finite-difference scheme

$$P_{j+1/2}\left(\frac{F_{j+1}-F_j}{h^2}\right)-P_{j-1/2}\left(\frac{F_j-F_{j-1}}{h^2}\right) \\ +(Q_j+\lambda^{\mathrm{m}}R_j)F_j=0, \qquad j=2,\ldots,N-1, \tag{11}$$

where integer (half-integer) subscripts denote evaluation on the full (half) mesh. The eigenvalue has been superscripted (with m for "matrix") to clarify the discussion of the algorithm in later sections. Integrability of the solution is ensured by imposing the boundary conditions

$$F_1=F_N=0. \tag{12}$$

Defining now a solution vector $\bar{F}^{\mathrm{m}}=(F_2,\ldots,F_{N-1})$, Eq. (11) is easily cast into matrix form,

$$A\cdot\bar{F}^{\mathrm{m}}=\lambda^{\mathrm{m}}\bar{F}^{\mathrm{m}}. \tag{13}$$

The components of the matrix A are given by

$$h^2A_{ij}=\delta_{i,j-1}\left(\frac{P_{j+3/2}}{R_j}\right)+\delta_{i,j+1}\left(\frac{P_{j+1/2}}{R_{j+1}}\right) \\ -\delta_{ij}\frac{P_{j+3/2}+P_{j+1/2}-h^2Q_{j+1}}{R_{j+1}}, \qquad i,j=1,\ldots,N-2. \tag{14}$$

In this form, the task of obtaining the spectrum of Eq. (1) is reduced to obtaining the eigenvalues of a $(N-2)\times(N-2)$ real nonsymmetric tridiagonal matrix. Interestingly enough, the nondiagonal cross products are strictly positive because of the positiveness of both R and P. This allows the use of a very fast algorithm. The lowest eigenvalue (or any other eigenvalue of the discrete part of the spectrum) is first bracketed using Gerschgorin's theorem [20] and then approximated using a combination of bisection and Newton-like methods, as is shown in Section 4. The eigenfunction $\bar{F}^{\mathrm{m}}$ is obtained by inverse iteration [15].

3.1.1. Symmetry points. For certain choices of the initial point $y=0$, the number of grid points required can be halved without losing accuracy in the calculation of the eigenvalue. In 3-D configurations with stellarator symmetry, a set of initial points exists for which the ballooning equation is symmetric under the transformation $y\to -y$. These points are of the form

$$(\theta_0,\zeta_0)=\left(l\pi,k\frac{\pi}{M}\right), \qquad l,k=0,1,\ldots, \tag{15}$$

with M the periodicity of the configuration. It is often the case that the most unstable ballooning modes are located at one of these positions. The integration domain can then be restricted to $[0,a]$, and solutions of a defined parity (even or odd) are sought. In this way, the lowest eigenvalue can be computed for roughly half as many grid points as in the nonsymmetric case. In terms of speed, it means an improvement of a factor of two (or possibly even more, since further computational efficiency is gained when evaluating the lowest eigenvalue of a matrix with a dimension half as large). Because the most unstable mode in this case is always an even eigenfunction [18], the following boundary conditions are used,

$$\left(\frac{\mathrm{d}F}{\mathrm{d}y}\right)_1 = F_N = 0. \tag{16}$$

As in the nonsymmetric case, the problem can be cast in the same matrix form given by Eq. (13), when including F_1 in the definition of $\bar{F}^{\mathrm{m}}$. The new $(N+1)/2 \times (N+1)/2$ real matrix A coefficients are now given by

$$h^2 A_{ij} = \begin{cases} 2\delta_{i,j-1}\left(\frac{P_{j-1}}{R_{j-1}}\right) - 2\delta_{ij}\frac{P_j}{R_j}, & i = 1,\ j = 1, \ldots, (N+1)/2 \\ \delta_{i,j-1}\left(\frac{P_{j+3/2}}{R_j}\right) + \delta_{i,j+1}\left(\frac{P_{j+1/2}}{R_{j+1}}\right) & \\ \quad - \delta_{ij}\frac{P_{j+3/2} + P_{j+1/2} - h^2 Q_{j+1}}{R_{j+1}}, & i, j = 2, \ldots, (N+1)/2. \end{cases} \tag{17}$$

It is important to note that in the nonsymmetric [symmetric] case, the spectrum of matrix A is discrete and contains, at most, $N-2\,[(N+1)/2]$ distinct eigenvalues, while the spectrum of Eq. (1) usually contains both discrete and continuous parts. The discreteness comes from the finite size of the numerical integration box, while the finite number of eigenvalues is due to the finite value of the grid step size h. Not surprisingly, Eq. (1) reduces to a standard Stürm–Liouville equation, with only a discrete spectrum containing infinitely many increasing real eigenvalues, when the domain is chosen to be the compact intervals $[-a, a]$ or $[0, a]$ [17]. As the value of h is reduced, Eq. (13) gives a better approximation of the first $N-2\,[(N+1)/2]$ eigenvalues of the Stürm–Liouville spectrum. When the domain is no longer compact, the discrete eigenvalues (if they exist at all) remain at the lower part of the spectrum. Therefore, choosing a sufficiently large compact domain provides a very good approximation of these lower eigenvalues, which correspond to the most unstable ballooning modes.

3.2. *Variational Refinement*

Using the second-order matrix scheme described in Subsection 3.1, a series of approximations to the actual eigenvalue is computed for increasingly finer meshes, with step sizes halved successively

$$h_k = \frac{h_0}{2^k}, \qquad k = 0, 1, \ldots, k_{\max}. \tag{18}$$

This relation is chosen to minimize the number of new Fourier inversions required at each step. Notice that in Eq. (11), the values of P, Q, and R on the full mesh at the $(k+1)$st iteration can be constructed without any further evaluation from their values on the full and half meshes at the kth iteration. The initial step size h_0 is usually chosen very large, corresponding to a coarse mesh. The step size reduction iteration terminates for iteration $k = k_{\max}$ when the extrapolation error falls below the specified tolerance (see Subsection 3.3).

When the matrix algorithm is used, the error in the eigenvalue is quadratic [14] in the mesh spacing,

$$\lambda^{\mathrm{m}} = \lambda_0 + \alpha h^2 + O(h^3). \tag{19}$$

The number of iterations needed for convergence can be reduced if the leading exponent in the power law in Eq. (19) can be increased. COBRA achieves this by refining the eigenvalue obtained at each iteration so that its dependence on the mesh step size becomes quartic, rather than quadratic. Because λ_0 is a minimum, the first variation of the functional given by Eq. (4) around the related eigenfunction F_0 must vanish. Suppose now that F_0 could somehow be approximated to order p accuracy,

$$F = F_0 + h^p \delta F + O(h^{p+1}), \qquad \delta F \sim O(1). \tag{20}$$

Inserting F into Eq. (4), it is straightforward to obtain

$$\lambda(F) = \lambda_0 - h^{2p} \left[\frac{\langle \delta F, L_0(y) - \lambda_0 R(y) \delta F \rangle}{\langle F, R(y) F \rangle} \right] + O(h^{2p+1}), \tag{21}$$

which is thus accurate to order $2p$.

Because the solution obtained from the matrix method, $\bar{F}^{\mathrm{m}}$, approximates the real solution to second order in h, inserting it into Eq. (4) thus gives a fourth order accurate approximation at each iteration,

$$\lambda^{\mathrm{v}} = \lambda_0 + \sigma h^4 + O(h^5). \tag{22}$$

Now the eigenvalue has been superscripted with v (“variational”) for clarity. Here, $\sigma > 0$, since λ_0 is a global minimum.

There is, however, a numerical subtlety related to the accuracy of the discretization chosen for the operator L_0 when λ^{v} is to be evaluated. If the same second order discretization scheme in Subsection 3.1 is used for L_0,

$$L_0 = L_0^{\mathrm{d}} + h^2 \delta L_0 + O(h^3), \qquad \delta L_0 \sim O(1), \tag{23}$$

then the numerical equivalent to Eq. (21), obtained by inserting $\bar{F}^{\mathrm{m}}$ in Eq. (4) and using L_0^{d} instead of L_0, becomes

$$\begin{aligned} \lambda(\bar{F}^{\mathrm{m}}) = \lambda_0 + h^2 &\left[\frac{\langle \bar{F}^{\mathrm{m}}, \delta L_0 \bar{F}^{\mathrm{m}} \rangle}{\langle \bar{F}^{\mathrm{m}}, R(y) \bar{F}^{\mathrm{m}} \rangle} \right] \\ &+ h^4 \left[\frac{2\langle \delta \bar{F}^{\mathrm{m}}, \delta L_0 \bar{F}^{\mathrm{m}} \rangle}{\langle \bar{F}^{\mathrm{m}}, R(y) \bar{F}^{\mathrm{m}} \rangle} - \frac{\left\langle \delta \bar{F}^{\mathrm{m}}, L_0^{\mathrm{d}}(y) - \lambda_0 R(y) \delta \bar{F}^{\mathrm{m}} \right\rangle}{\langle \bar{F}^{\mathrm{m}}, R(y) \bar{F}^{\mathrm{m}} \rangle} \right] + O(h^5). \end{aligned} \tag{24}$$

Notice the $O(h^2)$ term which dominates and thus masks the desired $O(h^4)$ scaling. To eliminate this term, it is necessary to use at least a fourth-order accurate discretization for L_0. Thus by introducing the higher-order discretization only in this variational formula, Eq. (24), the required scaling given by Eq. (22) is achieved without significantly increasing the computational time. In contrast, the efficiency of the algorithm would be critically affected if it were included in the matrix scheme (the matrix A would no longer be tridiagonal, and a different and slower technique would have to be used to compute λ^{m}).

3.3. *Richardson's Extrapolation*

The computational speed of the overall COBRA algorithm depends critically on the number of iterations to achieve convergence of the eigenvalue as $k \to \infty$ in Eq. (18). Every new iteration (k) increases the computational time by a factor of two. Because of the h^4 scaling of the varitional eigenvalue in Eq. (22) [in contrast to the h^2 scaling in Eq. (19)], it is possible to use Richardson's extrapolation [15] on a fairly coarse mesh to nevertheless obtain the $h_k \to 0$ limit, λ_0, of the eigenvalue. This scheme also provides an estimate of the extrapolation error, which is used to terminate the mesh sequencing as noted previously in Subsection 3.2.

3.4. *Integration Box Size*

The ballooning equation can also be transformed into a Schrödinger-like equation by changing to a new variable [17],

$$\tau(y) = \int_0^y \sqrt{R(s)/P(s)}\, \mathrm{d}s, \tag{25}$$

and by introducing a new dependent variable, H, defined as

$$H(\tau) \equiv [P(y(\tau))R(y(\tau))]^{1/4} F(y(\tau)). \tag{26}$$

The resulting Schrödinger-like equation takes the form

$$\frac{\mathrm{d}^2 H}{\mathrm{d}\tau^2} + [\lambda - V(\tau)]H = 0, \tag{27}$$

with the “ballooning potential,” V, given by

$$V(\tau) = -\left(\frac{Q}{R}\right) - \frac{3}{16}\left[\frac{\mathrm{d}(PR)/\mathrm{d}\tau}{PR}\right]^2 + \frac{1}{4}\left[\frac{\mathrm{d}^2(PR)/\mathrm{d}\tau^2}{PR}\right]. \tag{28}$$

Using the asymptotic behaviour of the ballooning coefficients (see Eq. (3)), it is easily verified that $V(\tau) \to 0$ when $y \to \pm\infty$, implying that solutions for $\lambda > 0$ are in the continuum part of the spectrum. For $\lambda < 0$, unstable ballooning modes can be localized in the potential well existing at $\tau = 0$ (if the well is sufficiently deep, see Fig. 1). The modes may

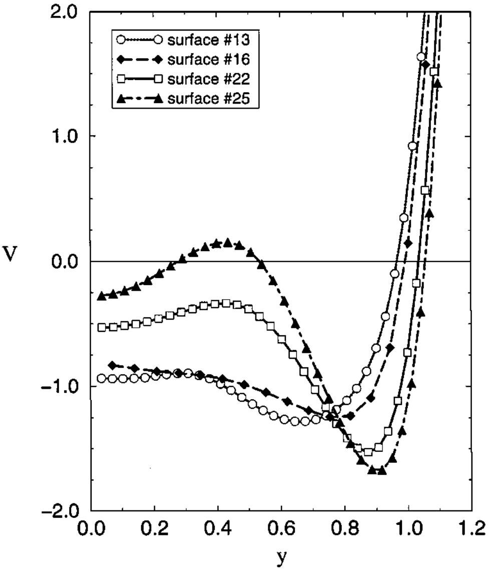

FIG. 1. Ballooning potential on different magnetic surfaces as a function of field line length y for the QOS equilibrium described in Section 4.

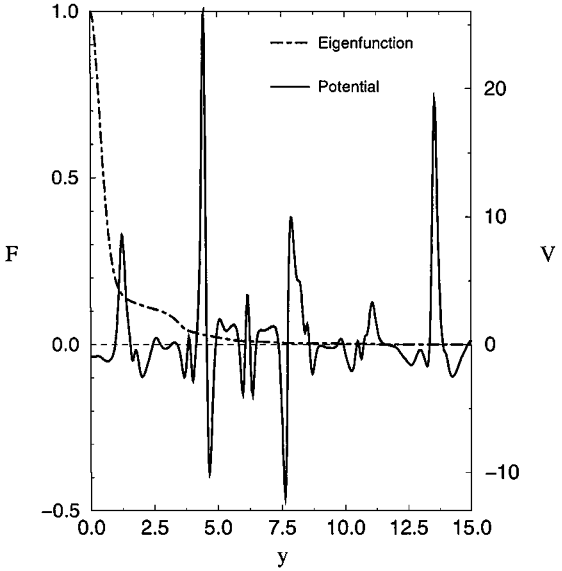

FIG. 2. Unstable eigenfunction and ballooning potential for the 13th surface.

also extend to nearby wells. These wells are separated by potential barriers (see Fig. 2) whose location along the magnetic field line strongly depends on the periodicity of the configuration, M, and the twist of the field line along the toroidal direction, characterized by ι, the ratio between the number of poloidal turns carried out during one toroidal turn. As a practical prescription, the location of the kth barrier can be roughly estimated as

$$y_{\text{barrier}}(k) \sim \frac{\pi}{M\iota}(2k-1), \qquad k = 1, 2, \ldots. \tag{29}$$

This prescription can be used to choose an appropriate value for a, the minimum size of the integration box, in the following way. Notice that when the mode extension goes beyond the first few barriers, the potential is no longer able to localize/destabilize the mode, which ceases to be integrable (it remains bounded, however, and becomes part of the continuous part of the spectrum). A typical case is shown in Fig. 3, where a nonlocalized (stable) mode escapes through the next barriers when the integration box size is increased. Since only unstable modes are of interest for the stability analysis, it is thus sufficient to set $a = y_{\text{barrier}}(k_w)$ with $k_w \gg 1$ in Eq. (29). In most COBRA runs, $k_w = 10$. Notice that this prescription implies that a changes at different magnetic surfaces, since ι usually varies from surface to surface due to magnetic shear.

4. NUMERICAL RESULTS

The main improvements included in COBRA with respect to the existing codes are Richardson's extrapolation scheme (RES), the variational refinement (VAR), and the use of symmetry. To numerically test these enhancements, some COBRA results are presented for an unstable QOS equilibrium configuration with periodicity $M = 3$, $\beta \simeq 2.5\%$, and containing 31 nested magnetic surfaces. Here, β is the volume-averaged measure of pressure. The number of modes used in the series representation for $|B|$, R, Z, and ρ is 829. The equilibrium is ballooning unstable all across the central region as shown in Fig. 4 (remember

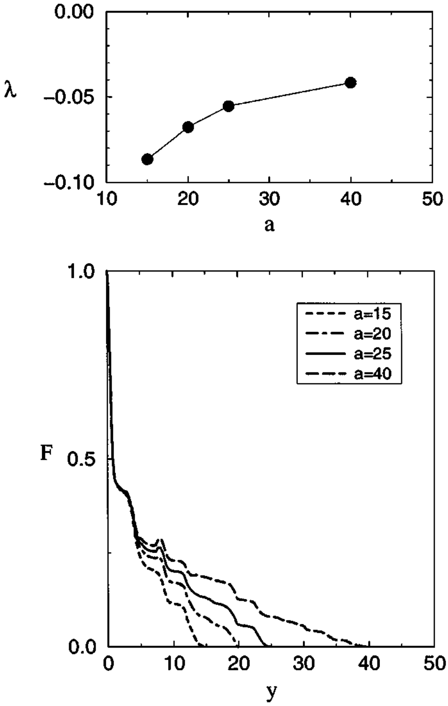

FIG. 3. Stable eigenfunction and ballooning potential for the 24th surface and increasing value of a. In the upper plot, the corresponding eigenvalue is shown.

that the growth rate is given by $\gamma^2 = -\lambda$). With respect to COBRA-specific parameters, all runs have been done setting the extrapolation error tolerance to 10^{-3}, the initial step size to $h_0 = 0.4$, and the box size is set with $k_w = 10$. All calculations have been performed on the CRAY C-90 at the National Energy Research Supercomputer Center (NERSC).

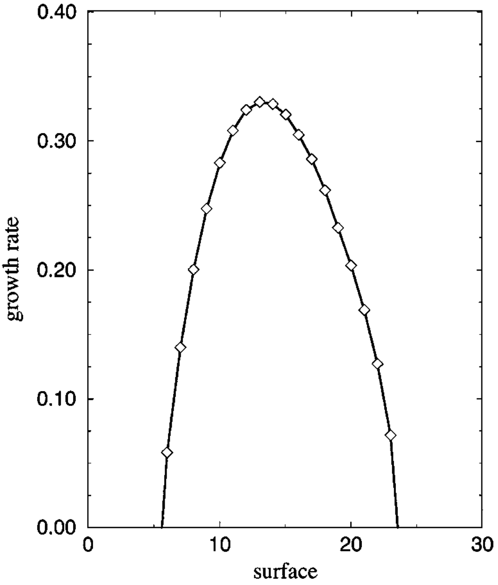

FIG. 4. Ballooning growth rate $\gamma = (-\lambda)^{1/2}$ normalized to the Alfvén time, $\tau_A \equiv \sqrt{\mu_0 \rho R_0^2 / B_0^2}$, ρ being the plasma mass density, R_0 the cylindrical major radius, and B_0 the magnetic field at the magnetic axis.

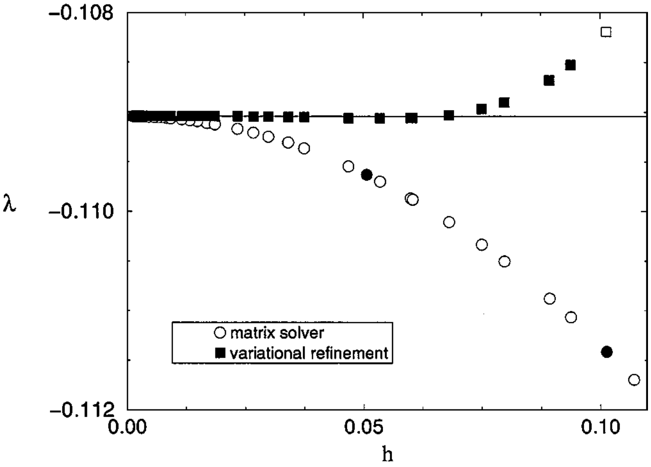

FIG. 5. Eigenvalue computed from the matrix scheme (open circles) and from the variational principle (VAR) (closed squares) as a function of the grid step-size h. The last few values used in the Richardson extrapolation (RES) are represented using distinctive symbols (respectively closed circles and open squares). All numerical values used in the extrapolation are listed in Table I.

To illustrate first how VAR works, both λ^{m} and λ^{v} are plotted versus the grid step size, h, in Fig. 5 for the 13th surface of the QOS equilibrium. The respective quadratic and quartic scalings can be clearly seen (the “exact” eigenvalue is also shown as a straight line for an easier comparison). Notice that the matrix scheme requires a mesh with a grid step size considerably finer to approximate the eigenvalue with accuracy comparable to that obtained with VAR. Using VAR reduces the number of iterations needed inside RES: the last few values of λ^{m} and λ^{v} that COBRA actually needs to respectively extrapolate the final eigenvalue from the matrix and variational values are also plotted in Fig. 5 using distinctive symbols (all of them are listed in Table I). Not surprisingly, the faster converging variational values allow extrapolation of the eigenvalue from a mesh that is twice as coarse (i.e., two times faster) for this particular case.

The performance and accuracy of COBRA compares advantageously with the ballooning codes currently in use. Both TERPSICHORE and 3DBALLOON rely on second-order accurate shooting algorithms with a fixed step size h_{f}. To compute the eigenvalue

TABLE I
Eigenvalue Convergence Sequence on the 13th Surface

	Richardson’s scheme					
	Matrix		Variational		Fixed step size	
	Asymmetric	Symmetric	Asymmetric	Symmetric	Asymmetric	Symmetric
$h_0 = 0.4$	−0.19247	−0.19426	0.09845	0.09876		
$h_1 = 0.2$	−0.11952	−0.11953	−0.09500	−0.09499		
$h_2 = 0.1$	−0.11142	−0.11142	−0.10819	−0.10819		
$h_3 = 0.05$	−0.10963	−0.10963				
$h_{\mathrm{f}} = 0.01$					−0.10945	−0.10945
$\lambda_{\text{extrapolated}}$	−0.10945	−0.10945	−0.10945	−0.10945		
$k_{\max}$	4	4	3	3		
CPU time(s)	0.4512	0.2268	0.2314	0.1247	1.8756	0.9465

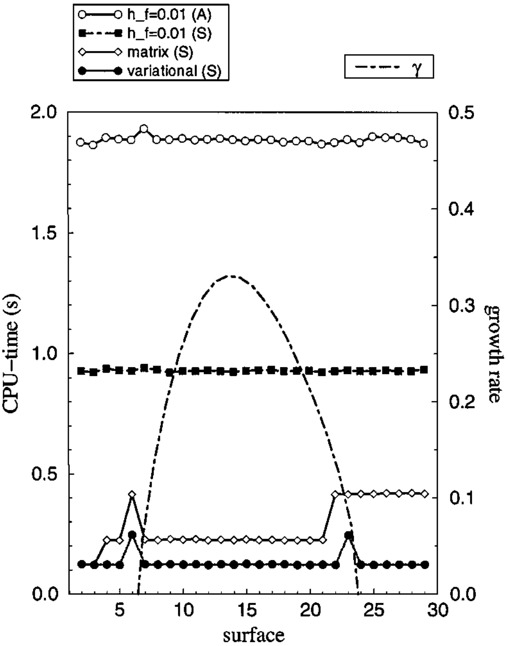

FIG. 6. CPU time required (left y-axis) to compute the ballooning growth rate from an initial symmetric point using: (a) RES coupled to the matrix solver (open diamonds); (b) RES coupled to VAR (closed circles); (c) a fixed step-size second-order shooting scheme (closed squares), and (d) the same as (c) but without using symmetry (open circles). Case (d) is equivalent to the approach of TERPSICHORE or 3DBALLOON. The growth rates are also included (right y-axis) to make apparent the finer meshes usually required for those modes which are close to becoming stable.

with accuracy comparable to COBRA, h_f must be chosen inside the "well-converged" region of the quadratic power law in Fig. 5 (typically, $h_\mathrm{f} \simeq 0.005 - 0.01$). This value is already five times smaller than the smallest step size that COBRA would need if the matrix scheme were used, and ten times smaller if VAR were considered. In Fig. 6, the CPU times required by the different methods are plotted together for a symmetric initial point choice. Notice how the use of symmetry allows a reduction of the time of the fixed step size scheme by a factor close to 2. When RES is coupled to the second-order solver, the CPU time is further reduced by a factor between 3 and 5, depending on the extension of the mode along the line. Finally, the total speed gain factor approaches 20 if VAR is considered because VAR's faster convergence is less sensitive to changes in the mode extension, as shown in Fig. 6. Also notice that without any extra computing time, convergence of the eigenvalue is guaranteed within this approach, while both TERPSICHORE and 3DBALLOON would require rerunning with a smaller step size to confirm this point.

There are other important advantages of this new approach as well. First, COBRA adapts the step size on different surfaces at run time to take into account the varying extension of the mode (notice that this is critical at those surfaces where the mode is close to becoming stable, as shown in Fig. 6). Second, the generality of the algorithm allows it to estimate in the same way any other eigenvalue of the discrete part of the spectrum of the ballooning equation. Even when 3DBALLOON can also evaluate all of them, it identifies the required eigenvalue by counting the computed eigenfunction zeros along the magnetic line (the eigenfunction associated to the kth eigenvalue must have $(k-1)$ zeros inside the integration interval [18]). However, this count can sometimes be rather sensitive because of the unexpected appearance, close to the boundaries of the interval, of numerical zeros caused by roundoff errors when k becomes large and the eigenvalue is close to the continuum.

ACKNOWLEDGMENTS

We are very grateful to B. A. Carreras, D. A. Spong, D. B. Batchelor, and J. F. Lyon for helpful comments and enlightening discussions, and to J. Lopez for constant encouragement. We are especially grateful to W. A. Cooper for providing us with the TERPSICHORE code, and to L. P. Ku and M. Redi for advise on its use. This research was sponsored by the U.S. Department of Energy, under Contract DE-AC05-96OR22464 with Lockheed Martin Energy Research Corp., and under Contract DE-FG0397ER54423 at the University of Montana. Research was supported in part (R.S.) by an appointment to the ORNL Postdoctoral Research Associates Program, administered jointly by Oak Ridge National Laboratory and the Oak Ridge Institute for Science and Education.

REFERENCES

1. S. P. Hirshman *et al.*, *Phys. Plasmas* **6**, 1858 (1999).
2. D. A. Spong *et al.*, Fusion energy 1998, in *Proc. 17th IAEA Conf., Yokohama, Japan, 1998*.
3. A. Reiman *et al.*, Fusion energy 1998, in *Proc. 17th IAEA Conf., Yokohama, Japan, 1998*.
4. J. R. Cary and S. G. Shasharina, *Phys. Rev. Lett.* **78**, 674 (1997).
5. S. P. Hirshman, W. I. Van Rij, and P. Merkel, *Comput. Phys. Comm.* **43**, 143 (1986).
6. S. P. Hirshman, D. A. Spong, J. C. Whitson, V. E. Lynch, D. B. Batchelor, B. A. Carreras, and J. A. Rome, *Phys. Rev. Lett.* **80**, 528 (1998).
7. D. A. Spong, S. P. Hirshman, J. C. Whitson, D. B. Batchelor, B. A. Carreras, V. E. Lynch, and J. A. Rome, *Phys. Plasmas* **5**, 1752 (1998).
8. D. Dobrott *et al.*, *Phys. Rev. Lett.* **39**, 943 (1977).
9. D. V. Anderson, W. A. Cooper, R. Gruber, S. Merazzi, and U. Schwenn, *J. Super Comput. Appl.* **4**, 34 (1990).
10. R. Sanchez, J. A. Jimenez, L. Garcia, and A. Varias, *Nucl. Fusion* **37**, 3557 (1997).
11. J. W. Connor, R. J. Hastie, and J. B. Taylor, *Proc. R. Soc. London A* **1**, 365 (1979).
12. D. Correa-restrepo, *Z. Naturforsch. A* **37**, 848 (1982).
13. R. L. Dewar and A. H. Glasser, *Phys. Fluids* **26**, 3038 (1983).
14. G. Dahlquist and A. Björck, *Numerical Methods* (Prentice Hall, Englewood Clifts, NJ, 1974).
15. W. Press, S. Teukolsky, W. Vettering, and B. Flannery, *Numerical Recipes* (Cambridge Univ. Press, Cambridge, MA, 1992).
16. A. H. Boozer, *Phys. Fluids* **23**, 904 (1980).
17. P. Morse and H. Fesbach, *Methods of Theoretical Physics* (McGraw–Hill, New York, 1953), VOl. I.
18. R. Courant and D. Hilbert, *Methods of Mathematical Physics* (Interscience, 1953. New York, 1953), Vol. I.
19. H. Sagan, *Introduction to the Calculus of Variations* (Dover, New York, 1969).
20. K. Rektorys, *Survey of Applicable Mathematics* (MIT Press, Cambridge, MA, 1969).